Cell Reports

Endogenous IGF Signaling Directs Heterogeneous Mesoderm Differentiation in Human Embryonic Stem Cells

Graphical Abstract

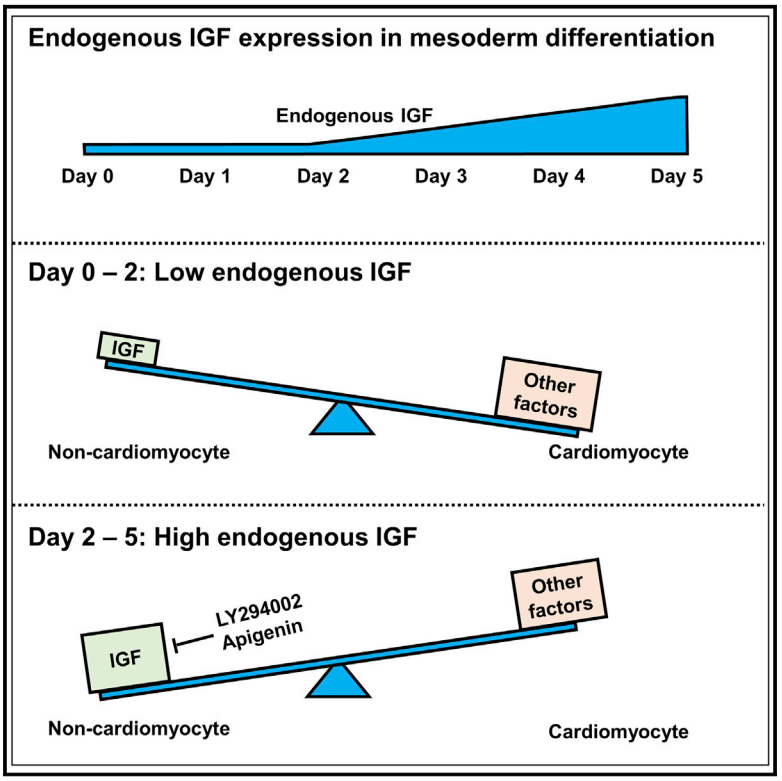

Highlights

- Exogenous insulin/IGF signal promotes heterogeneity in early mesoderm differentiation
- Endogenous IGF induced during mesoderm differentiation suppresses cardiomyocyte fate
- Inhibition of IGF pathway by LY294002 leads to effective cardiomyocyte differentiation
- LY294002 inhibits the CK2 pathway to promote cardiomyocyte cell fate

Authors

Yang Yang, Zhili Ren, Faxiang Xu, ..., Weiwei Liu, Wei Ge, Guokai Chen

Correspondence

guokaichen@um.edu.mo

In Brief

Yang et al. demonstrate that temporal regulation by insulin/IGF is essential for cell-type heterogeneity during human embryonic stem cell (hESC) differentiation. Inhibition of the endogenous IGF pathway promotes cardiomyocyte differentiation from mesoderm progenitors.

Yang et al., 2019, Cell Reports *29*, 3374–3384
December 10, 2019
https://doi.org/10.1016/j.celrep.2019.11.047

CellPress

OPEN ACCESS
CellPress

Cell Reports
Report

Endogenous IGF Signaling Directs Heterogeneous Mesoderm Differentiation in Human Embryonic Stem Cells

Yang Yang,[1] Zhili Ren,[1] Faxiang Xu,[1] Ya Meng,[1] Yumeng Zhang,[1] Nana Ai,[1] Yan Long,[1,2] Hio Ian Fok,[1,3] Chunhao Deng,[1] Xianyang Zhao,[4] Liancheng Huang,[5] Qi Zhao,[1] Jiaxian Wang,[6] Weiwei Liu,[1,3] Wei Ge,[1] and Guokai Chen[1,7,*]

[1]Centre of Reproduction, Development and Aging, Faculty of Health Sciences, University of Macau, Taipa, Macau
[2]Department of Cardiac Surgery, The First Affiliated Hospital of Sun Yat-sen University, Guangzhou, China
[3]Bioimaging and Stem Cell Core Facility, Faculty of Health Sciences, University of Macau, Taipa, Macau
[4]HELP Stem Cell Innovations Ltd. Co., Nanjing, China
[5]Guangzhou FulenGen Co., Ltd., Guangzhou, China
[6]Department of Cardiology, the First Affiliated Hospital of Nanjing Medical University, Nanjing, China
[7]Lead Contact
*Correspondence: guokaichen@um.edu.mo
https://doi.org/10.1016/j.celrep.2019.11.047

SUMMARY

During embryogenesis, various cell types emerge simultaneously from their common progenitors under the influence of intrinsic signals. Human embryonic stem cells can differentiate to diverse cell types of three embryonic lineages, making them an excellent system for understanding the regulatory mechanism that maintains the balance of different cell types in embryogenesis. In this report, we demonstrate that insulin-like growth factor (IGF) proteins are endogenously expressed during differentiation, and their temporal expression contributes to the cell fate diversity in mesoderm differentiation. Small molecule LY294002 inhibits the IGF pathway to promote cardiomyocyte differentiation while suppressing epicardial and noncardiac cell fates. LY294002-induced cardiomyocytes demonstrate characteristic cardiomyocyte features and provide insights into the molecular mechanisms underlying cardiac differentiation. We further show that LY294002 induces cardiomyocytes through CK2 pathway inhibition. This study elucidates the crucial roles of endogenous IGF in mesoderm differentiation and shows that the inhibition of the IGF pathway is an effective approach for generating cardiomyocytes.

INTRODUCTION

Human embryonic stem cells (hESCs) can self-renew without limits and are capable of generating all cell types in the human body, making them important models for understanding molecular mechanisms involved in human embryogenesis (Tabar and Studer, 2014; Thomson et al., 1998). Under the stimulation by different signals, various cell types can emerge from the same progenitor cells, and the proper balance of cell-type diversity is essential for a functional embryo (Burridge et al., 2012; Murry and Keller, 2008). Because signal transduction can be conveniently modulated with agonists and inhibitors in cell culture, hESCs provide an excellent platform for understanding the molecular mechanisms involved in cell fate specification and diversity in embryogenesis.

Without extrinsic stimuli, hESC differentiation is driven by intrinsic signals, and various cell types of three germ layers emerge spontaneously. It is interesting to understand what intrinsic signal is responsible for cell-type diversity under neutral conditions. For example, cardiomyocytes are among the various cell types that emerge through spontaneous differentiation (Kehat et al., 2001). However, some intrinsic signals must exist to prevent cells from all becoming cardiomyocytes. In developmental studies using mouse models, many signaling pathways such as BMP, WNT, and TGFβ are involved in embryonic heart development, and several key principles have been successfully applied in cardiac differentiation from hESCs (Burridge et al., 2012; Murry and Keller, 2008). Specific exogenous growth factors and small chemicals can effectively induce cardiomyocytes with high purity (Burridge et al., 2012, 2014). The WNT pathway is the main pathway in cardiac differentiation, and it is targeted by exogenous manipulation in cardiac production. WNT activation induces hESCs into mesoderm lineage, and the subsequent WNT activity level determines cardiomyocyte and non-cardiomyocyte cell fates. Continuous WNT activation induces epicardial cell fate (Witty et al., 2014), while WNT inhibition leads to cardiomyocytes (Batalov and Feinberg, 2015; Lian et al., 2012). It is unclear what endogenous factors modulate the balance of different signaling pathways to maintain the heterogenous population during spontaneous differentiation. Lian et al. (2013) show that after WNT activation, insulin suppresses BMP4/activin-induced cardiomyocyte differentiation. However, the WNT inhibitor curbs the insulin effect and promotes cardiomyocyte derivation (Lian et al., 2013), which suggests that the insulin signal is an upstream factor regulating cardiac cell fates in hESCs.

Insulin and insulin-like growth factors (IGFs) are essential for hESC maintenance (Chen et al., 2011; Wang et al., 2007), and

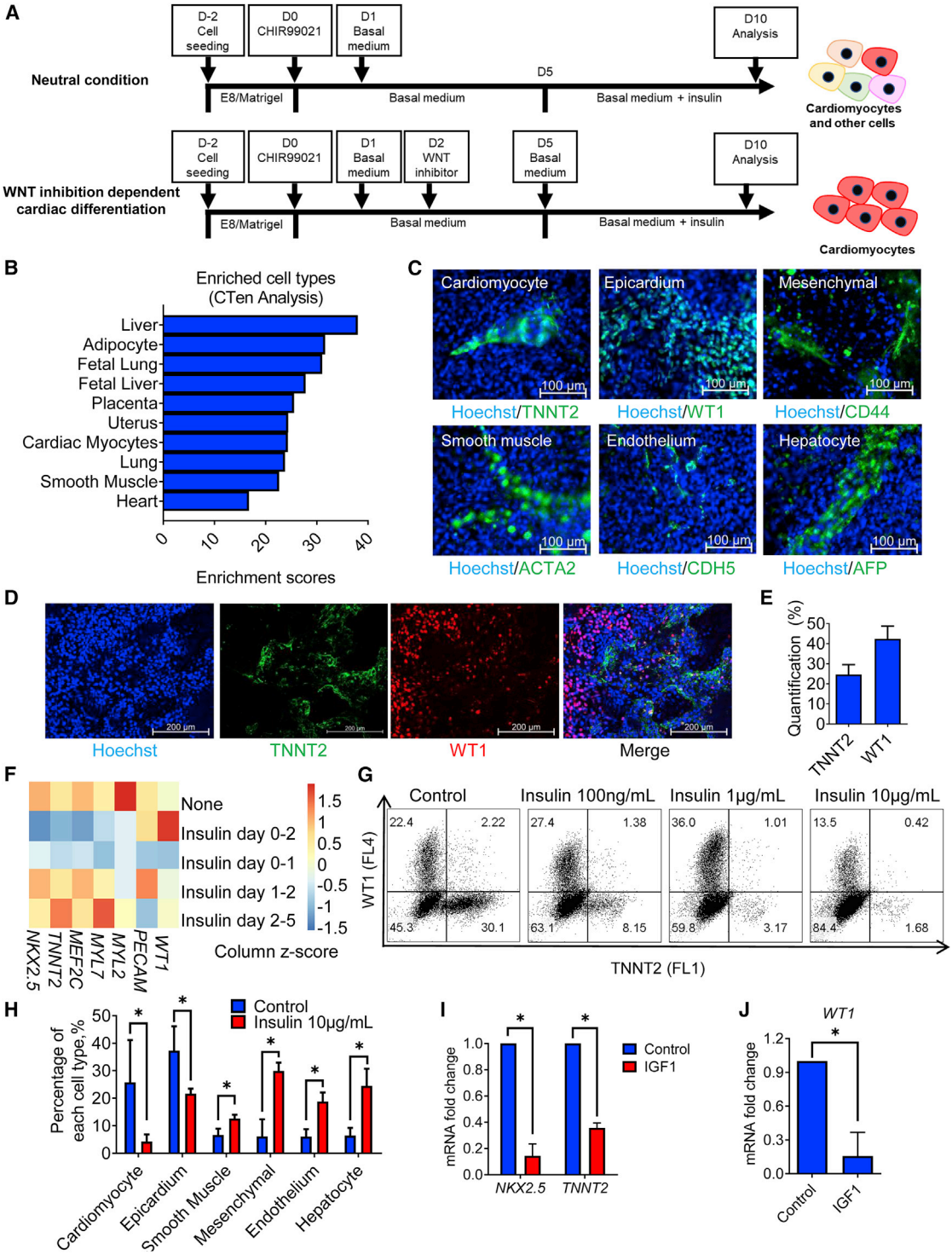

Figure 1. Insulin Promotes Cell-Type Diversity in Mesoderm Differentiation

(A) Diagram of differentiation strategies for mesoderm differentiation. hESCs were treated with GSK3 inhibitor CHIR99021 (5 μM) on day 0 for 24 h and then maintained under neutral conditions (basal medium only) or cardiomyocyte condition (IWP2 3 μM from day 2 to day 5). Cells were collected for further analysis on day 10.

(B) Cell-type enrichment analysis (CTen) to examine cell-type-specific differentiation. RNA from cells differentiated under neutral conditions were analyzed by microarray, and the global gene expression was compared against undifferentiated samples. Cell-type enrichment was determined according to the upregulated genes (≥2-fold) in differentiated cells.

(legend continued on next page)

at least one of them is present in all stem cell media (Akopian et al., 2010). In heterogeneous culture, hESC-derived niche cells secrete IGF proteins to sustain hESC renewal and survival (Bendall et al., 2007). Both insulin and IGFs bind to the insulin receptor or the IGF receptor to initiate downstream signal transduction, including the PI3K/AKT and casein kinase 2 (CK2) pathways (Boucher et al., 2010; Siddle, 2011). The PI3K/AKT cascade is often discussed in stem cell regulation. PI3K/AKT activation is essential to suppress caspase and cell death in hESC maintenance (Godoy-Parejo et al., 2019). During differentiation, the insulin/IGF activates the PI3K cascade to promote neuroectoderm lineage while suppressing endoderm cell fate determination (Yu and Cui, 2016). PI3K inhibitors are often utilized to modulate lineage-specific cell fate determination (Que et al., 2007; Roggia et al., 2007). Meanwhile, the insulin/IGF also stimulates WNT activity by increasing the phosphorylation of GSK3β at Ser9 (Lian et al., 2013). Besides the PI3K cascade, insulin/IGF signals also promote CK2 signaling by increasing its stability (Sommercorn et al., 1987; Wang et al., 1995). CK2 not only executes the signal transduction from the PI3K/AKT pathway (Borgo et al., 2017; Nguyen and Mitchell, 2013), but also contributes to WNT signaling through the regulation of dishevelled (DVL) and GSK3β (Seldin et al., 2005; Song et al., 2000). Even though these CK2-associated pathways are important for pluripotency and differentiation, CK2 function and application are rarely discussed in hESCs.

We are interested in the endogenous signals involved in the cell fate diversity during mesoderm differentiation, and we try to direct lineage-specific differentiation by modulating endogenous signaling pathways. We previously established an albumin-free, chemically defined differentiation procedure to induce cardiomyocytes (Lin et al., 2017), and we modified the procedure to establish a stimuli-free neutral condition, which was used to identify factors involved in the cell fate diversity during mesoderm differentiation (Figure 1A). In this report, we show that insulin/IGFs exert temporal regulation on mesoderm cell fates. Insulin suppresses cardiomyocyte differentiation during the induction of primitive streak while promoting the cell fate diversity of various mesoderm and endoderm cell types. During the cardiac specification stage, endogenous IGFs further inhibit the emergence of cardiomyocytes. The IGF pathway inhibitor LY294002 promotes cardiomyocyte differentiation and suppresses other cell types. We further show that CK2 inhibition by LY294002 suppresses DVL and GSK3β phosphorylation and contributes to cardiomyocyte differentiation. We then identified the CK2 inhibitor apigenin as an inducer for cardiomyocytes. This study identified the IGF as a critical signal maintaining the diversity of mesoderm cell fates, elucidated its molecular mechanism, and developed IGF and CK2 inhibition as alternative approaches to generate cardiomyocytes.

RESULTS

Insulin/IGFs Influence Cell Fate Diversity in Mesoderm Differentiation

In order to understand how endogenous signals direct cell fate decision among cardiomyocytes and other cell types, we used H1 hESCs to examine the emergence of different cell types in a growth-factor-free, neutral condition after WNT pathway activation by GSK3β inhibitor CHIR99021 (Figure 1A). Based on the microarray gene expression profile, according to cell-type enrichment analysis (CTen) (Shoemaker et al., 2012), multiple cell types emerged after the initial induction, including liver, lung, adipocyte, and heart cells (Figure 1B). Similar results were obtained by tissue expression analysis in DAVID (Huang et al., 2009) and the Enrichr (Chen et al., 2013; Kuleshov et al., 2016) database (Figure S1A). The cell-type heterogeneity was further confirmed by immunofluorescence, including cardiomyocytes (TNNT2), epicardium (WT1) Zhao et al., 2017, mesenchymal stem cells (CD44), smooth muscle cells (ACTA2), endothelium (VE-cadherin/CDH5) James et al., 2010, and hepatocytes (AFP) Loh et al., 2014 (Figure 1C). Among the heterogeneous cell types, cardiomyocytes and epicardium comprised the majority of the population (Figures 1D and 1E). We used this differentiation platform to study the intrinsic signals that contribute to cell fate heterogeneity.

Insulin was reported to inhibit activin/BMP4-induced cardiomyocyte differentiation (Lian et al., 2013), so we examined how an insulin signal temporally regulated cardiac fate in initiated differentiation. We found that a low dose of insulin (1 μg/ml) suppressed cardiomyocyte differentiation in a temporal-dependent manner. Brief exposure to insulin from day 0 to day 2 suppressed spontaneous cardiomyocyte differentiation most significantly

(C) Immunostaining showing cell-type diversity under neutral conditions. Cells were fixed on day 10 and then stained with antibodies against lineage-specific markers for cardiomyocyte (TNNT2), epicardium (WT1), mesenchymal stem cell (CD44), smooth muscle (ACTA2), endothelium (CDH5[VE-cadherin]), and hepatocyte (AFP). Hoechst indicates nuclei. Scale bar, 100 μm.

(D) Myocardial and epicardial differentiation under neutral conditions. TNNT2 and WT1 were detected by immunostaining with specific antibodies on day 10. Hoechst indicates nuclei. Scale bar, 200 μm.

(E) The quantification of (D). Data are collected from three representative images.

(F) Temporal influence of insulin (1 μg/ml) on cell-type diversity. In the neutral differentiation conditions, insulin was applied to cells at different time points, and RNA was harvested on day 10 for analysis of gene expression by qPCR. Myocardial markers, *NKX2.5*, *TNNT2*, *MEF2C*, *MYL7*, and *MYL2*; endothelial marker, *PECAM*; epicardial marker, *WT1*.

(G) Dosage-dependent effect of insulin on myocardial and epicardial differentiation. Under neutral conditions, different concentrations of insulin were applied to differentiating cells between day 0 and day 2, and cells were harvested on day 10 for flow cytometry. Myocardial marker, TNNT2 (Alexa 488); epicardial marker, WT1 (Alexa 647).

(H) The impact of a high dose of insulin (10 μg/mL) on cell heterogeneity. Insulin was applied from day 0 to day 2. The cells were harvested on day 10 for flowcytometric analysis. Data are presented as mean ± SD of three or more independent experiments.

(I) The impact of IGF1 on cardiomyocyte differentiation. H1 cells were differentiated under neutral conditions, and IGF1 (25 ng/ml) was applied to cells from day 0 to day 2. RNA was harvested for qPCR on day 10. The results were normalized to the expression levels in the untreated control. Data are presented as mean ± SD of three independent experiments.

(J) The impact of IGF1 on epicardial differentiation (same sample set as in I).

while increasing epicardial differentiation. When applied after day 2, insulin's inhibition on cardiomyocyte differentiation diminished (Figures 1F and S1B). We also demonstrated that the inhibitory effect of insulin was dose dependent. With an increased insulin concentration between day 0 and day 2, the cardiomyocyte population was suppressed more significantly (Figure 1G). Insulin increased the WT1-positive epicardial population at 100 ng/ml and 1 μg/ml. Interestingly, 10 μg/ml insulin suppressed both epicardial and cardiomyocyte populations, suggesting that most cells became noncardiac cells (Figure 1G). Further studies showed that 10 μg/ml insulin in the first 2 days significantly elevated the differentiation of noncardiac cells, including smooth muscle, mesenchymal, endothelial, and hepatic cells (Figures 1H and S1C).

Insulin and IGFs stimulate similar signaling pathways, so we examined whether exogenous IGF1 affected differentiation in the same way as insulin. IGF1 exposure in the first two days suppressed both cardiomyocyte and epicardial differentiation (Figures 1I and 1J). It suggests that IGFs and insulin act similarly in differentiation following initial WNT activation. These data indicate that the strength and timing of insulin/IGF signaling play critical roles in the balance of cardiac and noncardiac cell fates. Brief exposure to the insulin/IGF upon the initiation of differentiation can lead to dramatic changes in cell-type diversity at later stages.

The Inhibition of an Endogenous IGF by LY294002 Promotes Cardiac Differentiation

Considering that insulin is not expressed in mesoderm progenitor cells, we examined whether IGFs are expressed in hESCs during differentiation. *IGF1* and *IGF2* were expressed in hESCs. *IGF* expression levels increased after CHIR99021 treatment and were suppressed by WNT inhibition through IWP2 treatment (Figure 2A). The IGF precursor was detected by western blotting, and its level also continuously increased during differentiation (Figures 2B and S2A). These data indicate that the IGF pathway is actively regulated during mesoderm differentiation. Immunostaining analysis showed that the IGF and its downstream target, CK2α, were universally expressed in mesoderm progenitors and were not differentially expressed in specific progenitor subtypes, such as PDGFRα-positive or KDR-positive progenitor cells (Figures S2B and S2C).

In order to explore the function of an endogenous IGF, we examined whether interference of the IGF function could affect differentiation. The IGF level increased after day 2, so an IGF-neutralizing antibody was applied to the cells on day 2. The neutralizing antibody partially suppressed AKT phosphorylation (Figures 2C and S2D), and decreased the CK2α level (Figures 2D and S2E). These results suggest that cells are actively stimulated by endogenous IGFs during mesoderm differentiation. We then examined whether the inhibition of the IGF pathway between day 2 and day 5 could affect cardiac differentiation (Figure S2F). Cardiomyocyte differentiation was enhanced by the IGF-neutralizing antibody treatment from day 2 to day 5 (Figures 2E and S2G). However, the antibody impact was not strong, probably due to incomplete inhibition by the blocking antibody. In order to effectively suppress the IGF pathway, PI3K inhibitor LY294002 was applied to the cells between day 2 and day 5 (Figure S2F), and it significantly increased cardiomyocyte differentiation while suppressing epicardial and other noncardiac lineages (Figures 2F and S2H). We then used LY294002 to further interrogate how the IGF pathway is involved in cell fate determination. LY294002 was applied to hESCs at different time points. The exposure to LY294002 in the first 2 days had no effect on cardiac gene expression, but it significantly improved cardiac differentiation when applied from day 2 to day 5 (Figure 2G; Video S1). This temporal effect was consistent with increased IGF expression after day 2. When the increased IGF activity was suppressed by LY294002 between day 2 and day 5, more cardiomyocytes emerged.

Immunostaining shows that LY294002 significantly increased the TNNT2 and NKX2.5 dual-positive population (Figure 2H) and suppressed WT1-positive epicardium cells (Figure 2I). After extended culture, cardiac troponin T and α-actinin formed well-organized structures in LY294002-derived cardiomyocytes (Figure 2J). Besides H1, LY294002 also increased cardiomyocyte differentiation in H9 hESCs and NL-4 hiPSCs, even in the presence of insulin (Figure 2K). LY294002-treated cells demonstrated electrophysiological profiles of typical cardiomyocytes (Figures 2L and S2I). These data suggest that LY294002 treatment can effectively promote cardiomyocyte differentiation from CHIR99021-induced progenitor cells.

In order to examine whether IGF-related cardiac differentiation is evolutionarily conserved, we applied LY294002 to zebrafish embryos during embryogenesis. Fifty percent of zebrafish embryos exposed to LY294002 hatched with enlarged hearts (Figures S2J and S2L), 58% without intersomitic vessels (ISVs), and 75% without subintestinal vessels (SIV) (Figures S2K and S2L). This is consistent with our findings in hESCs that IGF inhibition promotes cardiomyocyte differentiation but suppresses other cell types, such as endothelium (Figure 2G). These data suggest that the role of IGF signaling in cardiomyocyte and endothelial cell fate determination may be conserved.

Characterization of LY294002-Induced Cardiomyocyte Differentiation

In order to understand how LY294002 influences cardiac cell fate, we examined stage-specific lineage markers in a time course. LY294002 did not affect the expression of early markers of cardiac and hematopoietic lineages, such as *PDGFRα*, *KDR*, or *TAL1*. The markers of the second heart field (*ISL1*) and first heart field (*TBX5*) were also not affected by LY294002. However, LY294002 significantly increased cardiac progenitor markers *NKX2.5* and *MEF2C* while decreasing endothelial (*PECAM*) and epicardial (*WT1* and *TBX18*) expression (Figure S3A). Based on the time course, we further examined the progenitors by flowcytometric analysis. We showed that IWP2 and LY294002 jointly enhanced MEF2C- and NKX2.5-positive populations on day 8 (Figures 3A–3C). Meanwhile, LY294002 suppressed endothelial differentiation (Figures 3D and S3B). These data suggest that the IGF suppresses cardiomyocyte fate during the transition from cardiac mesoderm to cardiac progenitors. The LY294002 and IWP-2 joint treatment did not show additive effects on TNNT2 expression (Figures 3E and S3C). This indicates that they probably share some common mechanism that finally determines cell fate.

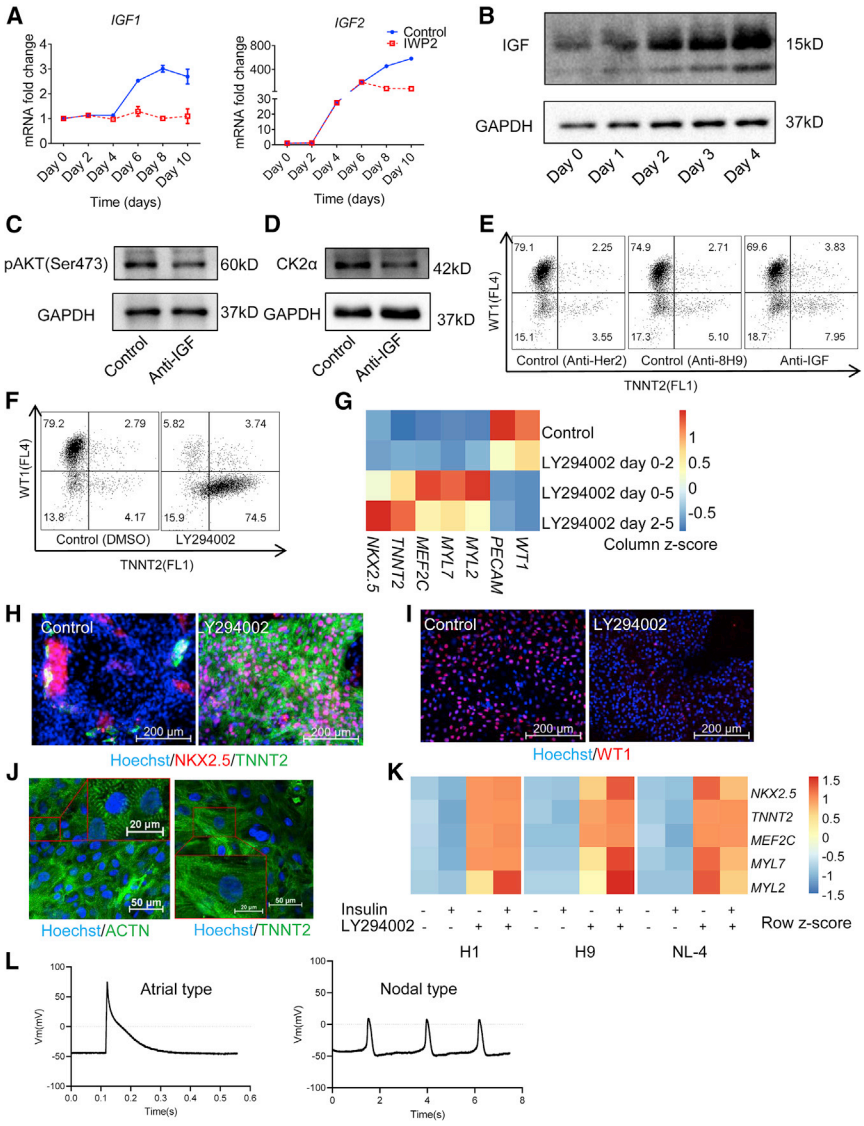

Figure 2. The Inhibition of the IGF Promotes Cardiomyocyte Differentiation

(A) The time course of *IGF1* and *IGF2* expression in neutral or IWP2-induced cardiac conditions. IWP2 was applied from day 2 to day 5. The cells were harvested at indicated time points for analysis of gene expression by qRT-PCR. The results were normalized to the expression levels in undifferentiated cells. Data are presented as mean ± SD of two technical repeats.

(B) Pro-IGF protein expression during differentiation. Under neutral conditions, proteins were harvested every day and then analyzed with an anti-IGF antibody in western blotting. GAPDH was used as an internal loading control. The quantification is in Figure S2A.

(C) Inhibition of AKT phosphorylation by an IGF antibody. An IGF-blocking antibody (300 nM) was applied to hESCs on day 2, and proteins were harvested after 24 h for western blotting with an anti-AKT (Ser473) antibody. The quantification is in Figure S2D.

(D) Inhibition of CK2α by IGF antibody, analyzed with anti-CK2α western blotting. The quantification is in Figure S2E.

(E) The impact of IGF inhibition on cardiomyocyte differentiation. An IGF-blocking antibody and anti-Her2 (control) and anti-8H9 (control) antibodies were applied separately to cells from day 2 to day5, and cells were harvested on day 10 for flow cytometry analysis. Myocardial marker, TNNT2 (Alexa 488); epicardial marker, WT1 (Alexa 647).

(F) The impact of LY294002 on cardiomyocyte differentiation. LY294002 (10 μM) and DMSO control were applied to cells separately from day 2 to day 5, and cells were harvested on day 10 for flow cytometry analysis.

(G) Temporal influence of IGF downstream inhibition by LY294002 on cardiomyocyte differentiation. LY294002 was used to block the IGF pathway at different time points, and cells were harvested on day 10 for qPCR.

(H) Immunostaining of LY294002-induced cells. hESCs were treated under neutral conditions or with LY294002 from day 2 to day 5 and were then fixed at day 10 and stained with antibodies against cardiac markers TNNT2 and NKX2.5. Scale bar, 200 μm.

(I) The same set of cells from (H) were fixed and stained with an antibody against epicardial marker WT1. Scale bar, 200 μm.

(J) Immunostaining of LY294002-induced cells after extended culture. LY294002-induced cells were passaged on day 10 and cultured for another 20 days, and then they were fixed and stained with anti-ACTN and TNNT2 antibodies. Scale bar, 50 μm and 20 μm (red box).

(K) The effect of LY294002 on cardiac differentiation in multiple cell lines. H1, H9, and NL-4 lines were treated with LY294002 from day 2 to day 5, and the cells were harvested on day 10 for analysis of gene expression by qRT-PCR.

(L) Representative action potential profiles from electrophysiological characterization of LY294002-induced cardiomyocytes.

We then compared the global gene expression of cardiomyocytes generated by LY294002 and IWP2 alone or in combination. The gene expression profile of LY294002-treated cells was clustered together with IWP2-treated cells, in comparison with control or insulin treatments (Figure 3F). LY294002 suppressed differentiation to non-myocardial lineages, including epicardium, smooth muscle, mesenchymal, endothelium, and hepatocyte, while enhancing cardiac genes (Figure 3G). CTen showed that LY294002-treated cells displayed a high enrichment of cardiomyocyte genes (Figures 3H and S3D). We further compared cardiomyocytes generated by IWP2 and IWP2+LY294002 treatments. The combination of IWP2 and LY294002 enhanced gene expression in lipid metabolism and mitochondrial functions, compared with IWP2 alone (Figures 3I and S3E). The expression of specific metabolic genes was elevated by LY294002 treatment (Figure S3F), which was confirmed by qRT-PCR (Figure S3G).

We further examined the metabolic profiles of cardiomyocytes derived from different treatments. We observed no significant difference in common metabolites by liquid chromatography–mass spectrometry (LC-MS) analysis of IWP2-, LY294002-, and IWP2+LY294002-derived cardiomyocytes (Figure S3H).

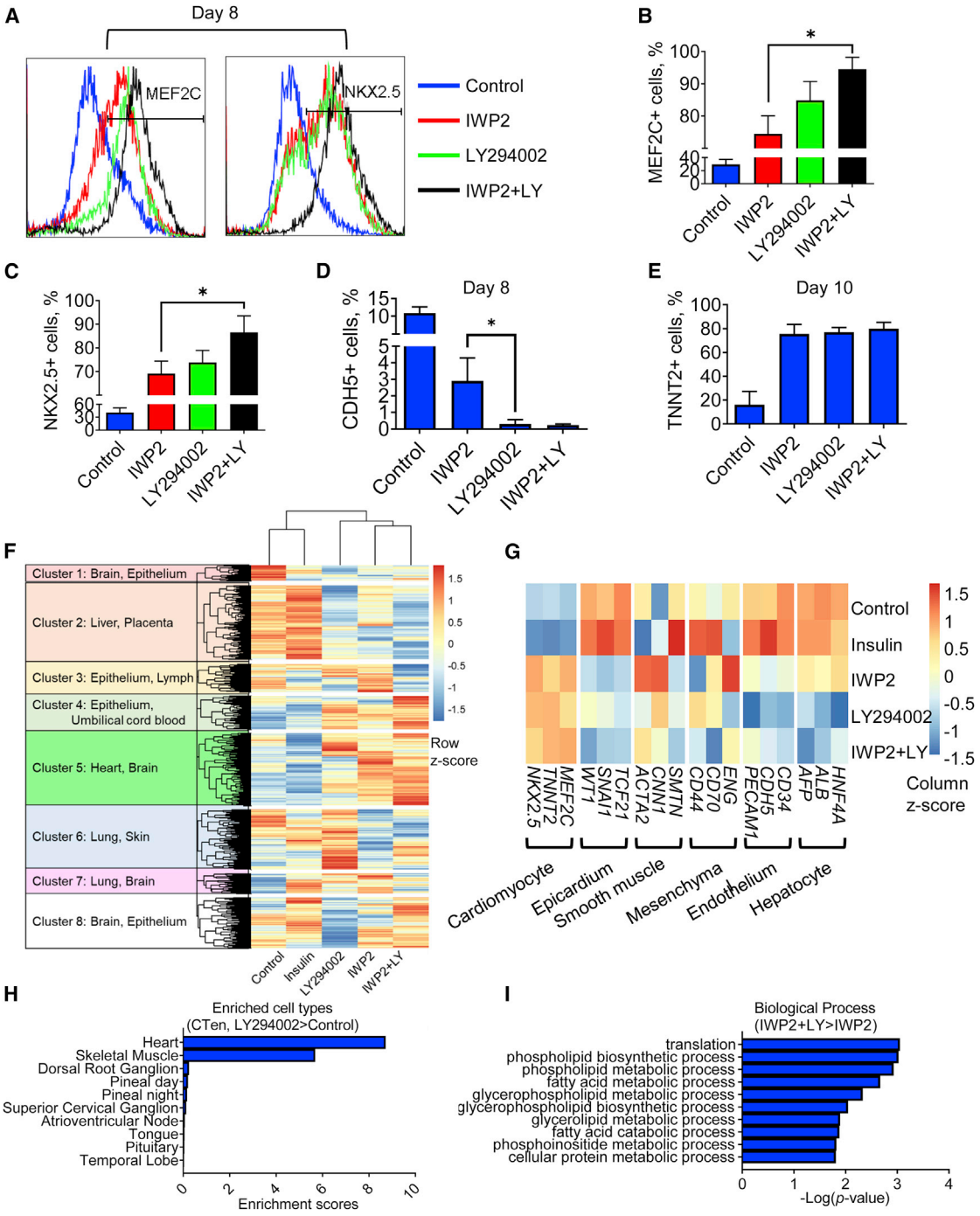

Figure 3. The Joint Effect of LY294002 and the WNT Inhibitor

(A) Impact of the joint treatment on cardiac progenitor yield. IWP2 and LY294002 were applied from day 2 to day 5. The cells were harvested on day 8 for flowcytometric analysis.

(B) The quantification of (A) (MEF2C-positive progenitors, n = 4 independent experiments).

(C) The quantification of (A) (NKX2.5-positive progenitors, n = 4 independent experiments).

(D) Impact of the joint treatment on endothelial yield. IWP2 and LY294002 were applied from day 2 to day 5. The cells were harvested on day 8 for flowcytometric analysis (n = 3 independent experiments).

(E) Impact of the joint treatment on cardiomyocyte yield. IWP2 and LY294002 were applied from day 2 to day 5. The cells were harvested on day 10 for flow-cytometric analysis. Data are presented as mean ± SD of three independent experiments.

(F) Cluster of global gene expression profiles from microarray analysis. H1 hESCs were treated with different conditions from day 2 to day 5, and RNA was harvested on day 10 for microarray analysis. David 6.7 was used to annotate the tissue specific expression of each cluster (https://david-d.ncifcrf.gov/).

(legend continued on next page)

Similar mitochondrial contents were observed in IWP2+ LY294002- and IWP2-derived cardiomyocytes based on MitoTracker staining (Figure S3I). Considering that mixed-cell or subcell types could emerge from different treatments, we examined whether cellular phenotypes could be affected by different culture conditions, including a regular basal medium condition and a glucose-free, lactate-containing condition (Figure S3J). When cells were maintained in a regular basal medium throughout the process, IWP2-derived cardiomyocytes demonstrated higher basal and maximal oxygen consumption rates (OCRs) than cells derived under the other two conditions, while LY294002-treated cells had the lowest maximal OCRs (Figure S3K). In contrast, all the cells showed similar OCR profiles in the glucose-free lactate medium. At the same time, we show that IWP2-induced cells have differential expressions of MYL7 and MYL2 compared to cells under LY294002-related treatments (Figure S3L). However, after a few days of treatment in the glucose-free lactate medium, the cells showed similar OCR profiles. These data suggest that the cells derived from different methods probably have the plasticity to change their gene expression and metabolic profile. Although different treatment leads to differential maturation gene expression on day 10 (Figure S3G), a similar maturation expression was observed after further culturing under both conditions (Figure S3M). It indicates that LY294002 treatment modulates the expression of some cardiac genes at early stage but does not impact the cardiac maturation process.

LY294002 Regulates Cardiac Differentiation through the CK2-Mediated WNT/β-Catenin Pathway

Because cardiac induction by IGF inhibition has not been reported before, we further examined the molecular mechanism of IGFs in cardiomyocyte differentiation. We found that the WNT inhibitor IWP2 induced cardiomyocyte differentiation in the presence of insulin (Figure 4A), suggesting that WNT signaling is downstream of the insulin/IGF pathway. We inspected whether IGF inhibition regulates the WNT pathway during cardiomyocyte differentiation. We found that non-phosphorylated β-catenin was decreased in LY294002-treated cells, implying that less β-catenin was available to translocate into the nucleus (Figures 4B and S4A). We then confirmed that nuclear β-catenin was indeed decreased in LY294002-treated cells, indicating less β-catenin was involved in transcription regulation in the nuclei (Figures 4C and S4B). These results suggest that LY294002 inhibits β-catenin activity and the WNT pathway.

LY294002 is usually used to inhibit the PI3K pathway, so we examined whether other common PI3K inhibitors could also induce cardiomyocytes. To our surprise, only PI103 demonstrated the potential to induce TNNT2-positive cells, while wortmannin did not have the ability (Figure 4D). This phenomenon was then confirmed by qPCR (Figure 4E). Western blotting showed that wortmannin suppressed AKT phosphorylation similarly to the LY294002 and PI103 treatments (Figures 4F and S4C). This suggests that in addition to PI3K/AKT inhibition, LY294002 and PI103 probably induced cardiomyocyte differentiation through another pathway.

It is reported that LY294002 can inhibit multiple targets in addition to PI3Ks (Gharbi et al., 2007), so we compared the target specificity of LY294002, PI103, and wortmannin according to the bioassay results from the PubChem database. All three compounds inhibited PI3K catalytic subunits α, β, γ, and δ (Figure 4G). At the same time, LY294002 and PI103 shared seven additional targets that were not inhibited by wortmannin (Figure 4G). Among the seven targets, two targets belong to the CK2 family (CK2α and CK2α′ subunits). We focused on these CK2 targets, because they are also downstream effectors of the IGF/insulin pathway. Western blotting showed that LY294002 and PI103 decreased the CK2α level, but wortmannin did not (Figures 4H and S4D). This confirmed that LY294002 and PI103 specifically inhibited CK2 in hESCs.

It was reported that CK2 promotes WNT pathway activity by stabilizing β-catenin through DVL (Song et al., 2000). We showed that LY294002, PI103, and CK2 inhibitor CX4945 decreased the DVL level, but wortmannin did not (Figures 4I and S4E–S4H). In contrast, all three PI3K inhibitors suppressed GSK3β phosphorylation that is affected by AKT (Figures 4I and S4F). These data suggest that PI103 and LY294002 suppressed the WNT pathway through CK2 inhibition, and wortmannin could not achieve similar effects due to its lack of a CK2 inhibitory effect.

Our results implied that LY294002 and PI103 induced cardiomyocyte differentiation through CK2 inhibition, so we tested whether common CK2 inhibitors could promote cardiac differentiation. We found that CX4945 increased cardiomyocyte differentiation (Figure 4J), but severe cell death was observed. We later found that cells were more tolerant to apigenin, another CK2 inhibitor. Apigenin decreased DVL in the same way as did LY294002 and CX4945 (Figures 4K and S4I). Apigenin significantly increased cardiomyocyte gene expression (Figure S4J) and the percentage of TNNT2-positive cells (Figure 4L).

We further examined CK2α function in hESCs by knocking down *CSNK2A1* with shRNA. Two independent shRNAs both significantly decreased *CSNK2A1* expression in 293FT cells and H1 hESCs (Figures S4K and S4L). However, the knockdown killed most hESCs within 48 h (Figure S4M), but not 293FT cells. This indicates that CK2 is essential for hESC survival, which is consistent with the CX4945 effect. We then performed *CSNK2A1* knockdown during differentiation. Lentiviral *CSNK2A1* shRNAs were applied to hESCs on day 2 during CHIR99021-induced differentiation under neutral conditions. When *CSNK2A1* was knocked down by shRNAs (Figure S4N), *NKX2.5* and *TNNT2* expression was increased in cells expressing shRNA (Figure S4O). These data support the notion that LY294002 promotes cardiac differentiation by inhibiting the CK2 pathway.

(G) Heatmap showing microarray analysis of the cell-type-specific gene expression with different treatments.
(H) CTen analysis on LY294002-treated cells. Global gene expression was compared between LY294002-treated cells and those maintained under neutral conditions. Cell-type enrichment was determined according to the upregulated genes (≥1.5-fold) in LY294002-treated cells.
(I) GO biological process enrichment for the upregulated genes of IWP2+LY294002-treated cells compared to IWP2-treated cells. Genes with at least 1.5-fold difference were included.

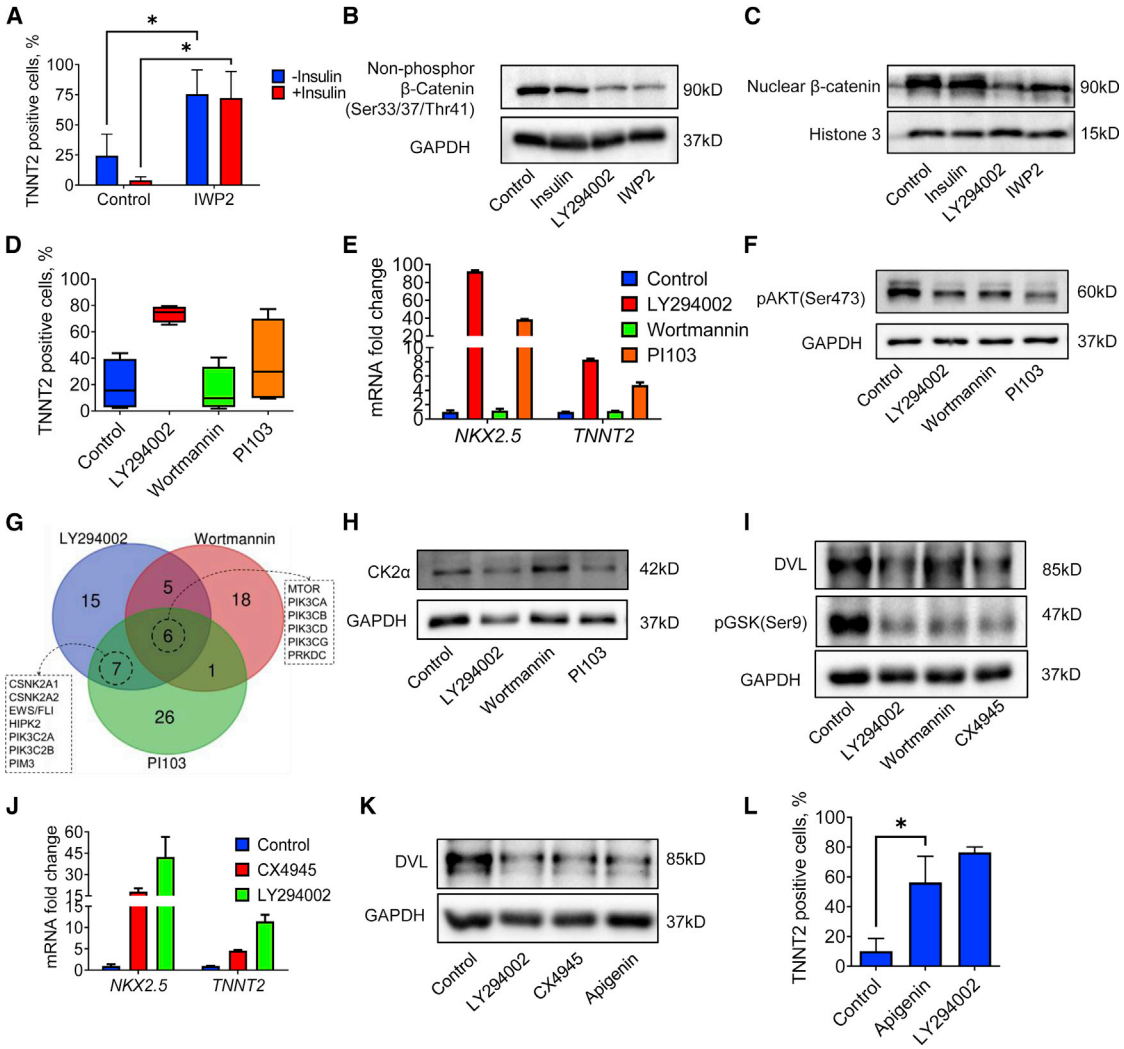

Figure 4. LY294002 Promotes Cardiac Differentiation through the CK2-Mediated WNT/β-Catenin Pathway

(A) WNT inhibitor IWP2 reversed insulin inhibition in cardiac differentiation. In total, 1 μg/mL insulin was added from day 0 to day 2, and IWP2 was added from day 2 to day 5. The cells were harvested on day 10 for flow cytometric analysis. Data are presented as mean ± SD of three independent experiments.

(B) Impact of insulin and LY294002 on the level of non-phospho-β-catenin (Ser33/37/Thr41) during differentiation. Insulin, IWP2, or LY294002 was applied to hESCs on day 2, and the whole-cell lysates were harvested after 24 h of treatment for western blot analysis of non-phospho-β-catenin. GAPDH was used as an internal loading control. The quantification is in Figure S4A.

(C) Impact of insulin and LY294002 on nuclear β-catenin. Insulin, IWP2, or LY294002 was applied to hESCs for 24 h on day 2, and nuclear fractions were isolated for western blot analysis. Histone 3 was used as an internal loading control. The quantification is in Figure S4B.

(D) Impact of different PI3K inhibitors on cardiomyocyte differentiation. hESCs were treated with LY294002, wortmannin (100 nM), or PI103 (100 nM) from day 2 to day 5, and cells were harvested on day 10 for flow cytometry analysis. Data represent four independent experiments.

(E) Impact of different PI3K inhibitors on TNNT2 expression. hESCs were treated with LY294002, wortmannin, or PI103 from day 2 to day 5, and the cells were harvested on day 10 for gene expression analysis by qPCR. Data are shown as mean ± SD of two technical repeats.

(F) Effect of different PI3K inhibitors on AKT (Ser473) phosphorylation. hESCs were treated with LY294002, wortmannin, or PI103 for 24 h on day 2, and whole-cell lysates were harvested for western blot analysis. GAPDH was used as an internal control. The quantification is in Figure S4C.

(G) Venn diagram of the specificity analysis of PI3K inhibitors LY294002 and PI103. The active targets of three PI3K inhibitors were identified according to the PubChem database.

(H) Inhibition of CK2α by different PI3K inhibitors. hESCs were treated with LY294002, wortmannin, or PI103 for 24 h on day 2, and whole-cell lysates were harvested for western blot analysis. GAPDH was used as an internal loading control. The quantification is in Figure S4D.

(I) Effect of LY294002, PI3K-specific inhibitor wortmannin, and CK2-specific inhibitor CX4945 on DVL and GSK3β (Ser9) phosphorylation. hESCs were treated with LY294002, wortmannin, or CX4945 for 24 h on day 2, and whole-cell lysates were harvested for analysis. GAPDH was used as an internal loading control. The quantification is in Figures S4E and S4F.

(J) Impact of CX4945 on cardiomyocyte marker *NKX2.5* and *TNNT2* expression. CX4945 (300 nM) was applied to hESCs for 24 h on day 2, and cells were harvested on day 10 for gene expression analysis by qRT-PCR. Data are presented as mean ± SD of two technical repeats and are representative of three independent experiments.

(legend continued on next page)

DISCUSSION

The balance of different growth factor signals leads to heterogeneous cell differentiation in the embryo. When the balance is broken, some specific cell types may dominate in the population and lead to failed embryogenesis (Allan et al., 2001; Eivers et al., 2004) Liu et al., 2018. In this study, we demonstrate that an endogenous IGF is essential for the cell-type diversity in mesodermal differentiation, and the inhibition of IGF signaling leads to cardiomyocyte cell fate.

The IGF and insulin activate the PI3K and CK2 cascades, and they are essential for hPSC maintenance (Bendall et al., 2007; Chen et al., 2011; Godoy-Parejo et al., 2019; Wang et al., 2007). This study reveals the temporal regulation of IGFs on mesodermal differentiation (Figure S4P). When hESCs are induced to differentiation by WNT activation, endogenous levels of the IGF are relatively low in the first 2 days, which allows some cells to be committed to cardiomyocytes in neutral culture conditions. If the IGF signal strength is increased at this stage, cardiomyocyte differentiation is suppressed, and noncardiomyocyte cell types increase significantly. After the day 0 to day 2 time window, endogenous IGF expression increases continuously in the progenitors and is sufficient to prevent uncommitted cells from becoming cardiomyocytes, resulting in a diverse cell population. By suppressing the IGF pathway with LY294002, the signaling balance is shifted to promote cardiomyocyte differentiation. As an upstream regulator of WNT signaling, it is conceivable that endogenous IGF signaling serves as a key player in cardiac differentiation and development. It has been shown that a defective IGF pathway leads to an enlarged heart in early embryogenesis in mouse and zebrafish models (Hartnett et al., 2010; Lou et al., 2008). These findings are consistent with our results that the IGF controls cardiac differentiation on the hESC platform. Besides LY294002's role in cardiac differentiation, it also has significant impacts on endodermal induction and smooth muscle differentiation (Cheung et al., 2012; McLean et al., 2007). These facts imply that an endogenous IGF plays additional roles in cell fate determination during embryogenesis, and the IGF's regulatory mechanism in differentiation is still to be further elucidated.

Although cardiomyocytes can be efficiently derived with the WNT inhibitor and other modulators (Batalov and Feinberg, 2015; Lin et al., 2017), there are still many areas for improvement in cardiac differentiation and maturation. The IGF regulates not only the WNT pathway, but also metabolism and other important cellular activities (Chitnis et al., 2008; Freund et al., 1993). It is reasonable to speculate that cardiomyocytes induced by IGF inhibition may have different gene expression and metabolic profiles when compared with the cells generated by WNT inhibition. Our microarray data show that LY294002+IWP2 dual treatment leads to a distinctive gene expression profile in comparison to IWP2 alone (Figure S3F). LY294002-induced cells demonstrate differential metabolic profiles in the Seahorse analysis and differential expression of MYL2/MYL7 (Figures S3K and S3L), but the difference is diminished by maintenance in a glucose-free lactate medium. It suggests that cardiomyocytes from different methods have the plasticity for further changes. More studies are necessary to explore whether IGF manipulation could alter cardiomyocyte properties or improve cardiomyocyte quality for future applications.

In this report, we also made an interesting discovery regarding LY294002-modulated pathways. When LY294002 is applied to interrogate signal transduction, it is often considered as a PI3K inhibitor (Nie et al., 2017; Shu et al., 2018; Wu et al., 2015). We reveal that LY294002 inhibits not only PI3K, but also CK2 in cardiac differentiation. Particularly, LY294002 contributes to cardiomyocyte differentiation through CK2 inhibition. We inspected whether a similar phenomenon exists in other situations and found that LY294002 also functions through CK2 in other processes. For example, LY294002 has a strong effect on activin-induced endoderm differentiation (McLean et al., 2007; Singh et al., 2012), but we found that wortmannin could not improve endoderm differentiation as strongly. In contrast, the combination of the PI3K inhibitor wortmannin and the CK2 inhibitor CX4945 synergistically stimulated SOX17 expression similar to LY294002 (Figures S4Q and S4R). This suggests that LY294002 regulates endoderm differentiation partially through the CK2 pathway as well. This study provides another angle to appreciate the molecular mechanisms underlying LY294002 treatments.

In summary, we revealed the temporal regulation of endogenous IGFs that maintains the balance between cardiomyocyte and noncardiomyocyte cell fates in hESC differentiation. By modulating the IGF and CK2 pathways, two alternative cardiomyocyte differentiation methods are developed that complement conventional methods in cardiomyocyte production.

STAR★METHODS

Detailed methods are provided in the online version of this paper and include the following:

- KEY RESOURCES TABLE
- LEAD CONTACT AND MATERIALS AVAILABILITY
- EXPERIMENTAL MODEL AND SUBJECT DETAILS
  - Ethics Statement
  - Cell Lines
  - Zebrafish
- METHOD DETAILS
  - Mesoderm induction and subsequent differentiation
  - Endoderm differentiation
  - Reverse transcription and real-time quantitative PCR
  - Western blot
  - Flowcytometric analysis

(K) Impact of CK2 inhibitor apigenin on DVL level during differentiation. Apigenin (10 μM) was applied to hESCs for 24 h on day 2, and proteins were harvested for western blot analysis. GAPDH was used as an internal loading control. LY294002 and CX4945 were also used as positive controls. The quantification is in Figure S4I.

(L) Impact of apigenin on cardiomyocyte differentiation. hESCs were treated with apigenin from day 2 to day 5, and the cells were harvested on day 10 for flow cytometry. Data are presented as mean ± SD of three independent experiments.

SUPPLEMENTAL INFORMATION

Supplemental Information can be found online at https://doi.org/10.1016/j.celrep.2019.11.047.

ACKNOWLEDGMENTS

This work was supported by the Science and Technology Development Fund of Macau SAR (FDCT/131/2014/A3, FDCT/056/2015/A2, and FDCT/0059/2019/A1) and University of Macau Multiyear research grants (MYRG2015-00229-FHS and MYRG2018-00135-FHS).

AUTHOR CONTRIBUTIONS

G.C. and Y.Y. conceived and designed the study. Y.Y., Y.L., and G.C. examined insulin/IGF impacts on cardiac differentiation. Y.Y., Y.L., Y.M., W.L., and Z.R. performed hESC maintenance and differentiation. Y.Y. and Q.Z. examined IGF antibody function on differentiation. Z.R. and Y.Y. analyzed gene expression with the microarray. F.X., H.I.F., and Y.Y. analyzed the metabolic profile by LC-MS. Y.Z. conducted endodermal differentiation. Y.L., J.W., and X.Z. performed the electrophysiological analysis. N.A. and W.G. examined the LY294002 function on zebrafish development. Y.Y. and L.H. performed *CSNK2A1* knockdown experiments. Y.Y., W.L., and G.C. wrote the manuscript.

DECLARATION OF INTERESTS

Y.Y. and G.C. filed a patent application based on cardiomyocyte differentiation that is induced by inhibitors of IGF and CK2 pathways.

Received: December 4, 2018
Revised: September 23, 2019
Accepted: November 12, 2019
Published: December 10, 2019

REFERENCES

Ahmed, M., Cheng, M., Zhao, Q., Goldgur, Y., Cheal, S.M., Guo, H.F., Larson, S.M., and Cheung, N.K. (2015). Humanized Affinity-matured Monoclonal Antibody 8H9 Has Potent Antitumor Activity and Binds to FG Loop of Tumor Antigen B7-H3. J. Biol. Chem. *290*, 30018–30029.

Ai, N., Chong, C.M., Chen, W., Hu, Z., Su, H., Chen, G., Lei Wong, Q.W., and Ge, W. (2018). Ponatinib exerts anti-angiogenic effects in the zebrafish and human umbilical vein endothelial cells via blocking VEGFR signaling pathway. Oncotarget *9*, 31958–31970.

Akopian, V., Andrews, P.W., Beil, S., Benvenisty, N., Brehm, J., Christie, M., Ford, A., Fox, V., Gokhale, P.J., Healy, L., et al.; International Stem Cell Initiative Consortium (2010). Comparison of defined culture systems for feeder cell free propagation of human embryonic stem cells. In Vitro Cell. Dev. Biol. Anim. *46*, 247–258.

Allan, G.J., Flint, D.J., and Patel, K. (2001). Insulin-like growth factor axis during embryonic development. Reproduction *122*, 31–39.

Batalov, I., and Feinberg, A.W. (2015). Differentiation of Cardiomyocytes from Human Pluripotent Stem Cells Using Monolayer Culture. Biomark. Insights *10*, 71–76.

Beers, J., Gulbranson, D.R., George, N., Siniscalchi, L.I., Jones, J., Thomson, J.A., and Chen, G. (2012). Passaging and colony expansion of human pluripotent stem cells by enzyme-free dissociation in chemically defined culture conditions. Nat. Protoc. *7*, 2029–2040.

Bendall, S.C., Stewart, M.H., Menendez, P., George, D., Vijayaragavan, K., Werbowetski-Ogilvie, T., Ramos-Mejia, V., Rouleau, A., Yang, J., Bossé, M., et al. (2007). IGF and FGF cooperatively establish the regulatory stem cell niche of pluripotent human cells in vitro. Nature *448*, 1015–1021.

Borgo, C., Milan, G., Favaretto, F., Stasi, F., Fabris, R., Salizzato, V., Cesaro, L., Belligoli, A., Sanna, M., Foletto, M., et al. (2017). CK2 modulates adipocyte insulin-signaling and is up-regulated in human obesity. Sci. Rep. *7*, 17569.

Boucher, J., Tseng, Y.H., and Kahn, C.R. (2010). Insulin and insulin-like growth factor-1 receptors act as ligand-specific amplitude modulators of a common pathway regulating gene transcription. J. Biol. Chem. *285*, 17235–17245.

Burridge, P.W., Keller, G., Gold, J.D., and Wu, J.C. (2012). Production of de novo cardiomyocytes: human pluripotent stem cell differentiation and direct reprogramming. Cell Stem Cell *10*, 16–28.

Burridge, P.W., Matsa, E., Shukla, P., Lin, Z.C., Churko, J.M., Ebert, A.D., Lan, F., Diecke, S., Huber, B., Mordwinkin, N.M., et al. (2014). Chemically defined generation of human cardiomyocytes. Nat. Methods *11*, 855–860.

Chen, G., Gulbranson, D.R., Hou, Z., Bolin, J.M., Ruotti, V., Probasco, M.D., Smuga-Otto, K., Howden, S.E., Diol, N.R., Propson, N.E., et al. (2011). Chemically defined conditions for human iPSC derivation and culture. Nat. Methods *8*, 424–429.

Chen, G., Gulbranson, D.R., Yu, P., Hou, Z., and Thomson, J.A. (2012). Thermal stability of fibroblast growth factor protein is a determinant factor in regulating self-renewal, differentiation, and reprogramming in human pluripotent stem cells. Stem Cells *30*, 623–630.

Chen, E.Y., Tan, C.M., Kou, Y., Duan, Q., Wang, Z., Meirelles, G.V., Clark, N.R., and Ma'ayan, A. (2013). Enrichr: interactive and collaborative HTML5 gene list enrichment analysis tool. BMC Bioinformatics *14*, 128.

Cheung, C., Bernardo, A.S., Trotter, M.W., Pedersen, R.A., and Sinha, S. (2012). Generation of human vascular smooth muscle subtypes provides insight into embryological origin-dependent disease susceptibility. Nat. Biotechnol. *30*, 165–173.

Chitnis, M.M., Yuen, J.S., Protheroe, A.S., Pollak, M., and Macaulay, V.M. (2008). The type 1 insulin-like growth factor receptor pathway. Clin. Cancer Res. *14*, 6364–6370.

Dignam, J.D., Lebovitz, R.M., and Roeder, R.G. (1983). Accurate transcription initiation by RNA polymerase II in a soluble extract from isolated mammalian nuclei. Nucleic Acids Res. *11*, 1475–1489.

Eivers, E., McCarthy, K., Glynn, C., Nolan, C.M., and Byrnes, L. (2004). Insulin-like growth factor (IGF) signalling is required for early dorso-anterior development of the zebrafish embryo. Int. J. Dev. Biol. *48*, 1131–1140.

Freund, G.G., Kulas, D.T., and Mooney, R.A. (1993). Insulin and IGF-1 increase mitogenesis and glucose metabolism in the multiple myeloma cell line, RPMI 8226. J. Immunol. *151*, 1811–1820.

Gharbi, S.I., Zvelebil, M.J., Shuttleworth, S.J., Hancox, T., Saghir, N., Timms, J.F., and Waterfield, M.D. (2007). Exploring the specificity of the PI3K family inhibitor LY294002. Biochem. J. *404*, 15–21.

Godoy-Parejo, C., Deng, C., Liu, W., and Chen, G. (2019). Insulin Stimulates PI3K/AKT and Cell Adhesion to Promote the Survival of Individualized Human Embryonic Stem Cells. Stem Cells *37*, 1030–1041.

Gustafsson Sheppard, N., Jarl, L., Mahadessian, D., Strittmatter, L., Schmidt, A., Madhusudan, N., Tegnér, J., Lundberg, E.K., Asplund, A., Jain, M., and Nilsson, R. (2015). The folate-coupled enzyme MTHFD2 is a nuclear protein and promotes cell proliferation. Sci. Rep. *5*, 15029.

Harries, M., and Smith, I. (2002). The development and clinical use of trastuzumab (Herceptin). Endocr. Relat. Cancer *9*, 75–85.

Hartnett, L., Glynn, C., Nolan, C.M., Grealy, M., and Byrnes, L. (2010). Insulin-like growth factor-2 regulates early neural and cardiovascular system development in zebrafish embryos. Int. J. Dev. Biol. *54*, 573–583.

Huang, W., Sherman, B.T., and Lempicki, R.A. (2009). Systematic and integrative analysis of large gene lists using DAVID bioinformatics resources. Nat. Protoc. *4*, 44–57.

James, D., Nam, H.S., Seandel, M., Nolan, D., Janovitz, T., Tomishima, M., Studer, L., Lee, G., Lyden, D., Benezra, R., et al. (2010). Expansion and maintenance of human embryonic stem cell-derived endothelial cells by TGFbeta inhibition is Id1 dependent. Nat. Biotechnol. *28*, 161–166.

Kehat, I., Kenyagin-Karsenti, D., Snir, M., Segev, H., Amit, M., Gepstein, A., Livne, E., Binah, O., Itskovitz-Eldor, J., and Gepstein, L. (2001). Human embryonic stem cells can differentiate into myocytes with structural and functional properties of cardiomyocytes. J. Clin. Invest. *108*, 407–414.

Kuleshov, M.V., Jones, M.R., Rouillard, A.D., Fernandez, N.F., Duan, Q., Wang, Z., Koplev, S., Jenkins, S.L., Jagodnik, K.M., Lachmann, A., et al. (2016). Enrichr: a comprehensive gene set enrichment analysis web server 2016 update. Nucleic Acids Res. *44*, W90-7.

Lian, X., Hsiao, C., Wilson, G., Zhu, K., Hazeltine, L.B., Azarin, S.M., Raval, K.K., Zhang, J., Kamp, T.J., and Palecek, S.P. (2012). Robust cardiomyocyte differentiation from human pluripotent stem cells via temporal modulation of canonical Wnt signaling. Proc. Natl. Acad. Sci. USA *109*, E1848–E1857.

Lian, X., Zhang, J., Zhu, K., Kamp, T.J., and Palecek, S.P. (2013). Insulin inhibits cardiac mesoderm, not mesendoderm, formation during cardiac differentiation of human pluripotent stem cells and modulation of canonical Wnt signaling can rescue this inhibition. Stem Cells *31*, 447–457.

Lin, Y., Linask, K.L., Mallon, B., Johnson, K., Klein, M., Beers, J., Xie, W., Du, Y., Liu, C., Lai, Y., et al. (2017). Heparin Promotes Cardiac Differentiation of Human Pluripotent Stem Cells in Chemically Defined Albumin-Free Medium, Enabling Consistent Manufacture of Cardiomyocytes. Stem Cells Transl. Med. *6*, 527–538.

Liu, W., Ren, Z., Lu, K., Song, C., Cheung, E.C.W., Zhou, Z., and Chen, G. (2018). The Suppression of Medium Acidosis Improves the Maintenance and Differentiation of Human Pluripotent Stem Cells at High Density in Defined Cell Culture Medium. Int. J. Biol. Sci. *14*, 485–496.

Loh, K.M., Ang, L.T., Zhang, J., Kumar, V., Ang, J., Auyeong, J.Q., Lee, K.L., Choo, S.H., Lim, C.Y., Nichane, M., et al. (2014). Efficient endoderm induction from human pluripotent stem cells by logically directing signals controlling lineage bifurcations. Cell Stem Cell *14*, 237–252.

Long, Y., Lin, Z., Xia, M., Zheng, W., and Li, Z. (2013). Mechanism of HERG potassium channel inhibition by tetra-n-octylammonium bromide and benzethonium chloride. Toxicol. Appl. Pharmacol. *267*, 155–166.

Lou, D.Y., Dominguez, I., Toselli, P., Landesman-Bollag, E., O'Brien, C., and Seldin, D.C. (2008). The alpha catalytic subunit of protein kinase CK2 is required for mouse embryonic development. Mol. Cell. Biol. *28*, 131–139.

McLean, A.B., D'Amour, K.A., Jones, K.L., Krishnamoorthy, M., Kulik, M.J., Reynolds, D.M., Sheppard, A.M., Liu, H., Xu, Y., Baetge, E.E., and Dalton, S. (2007). Activin a efficiently specifies definitive endoderm from human embryonic stem cells only when phosphatidylinositol 3-kinase signaling is suppressed. Stem Cells *25*, 29–38.

Murry, C.E., and Keller, G. (2008). Differentiation of embryonic stem cells to clinically relevant populations: lessons from embryonic development. Cell *132*, 661–680.

Nguyen, X.T., and Mitchell, B.S. (2013). Akt activation enhances ribosomal RNA synthesis through casein kinase II and TIF-IA. Proc. Natl. Acad. Sci. USA *110*, 20681–20686.

Nie, Y., Zhang, K., Zhang, S., Wang, D., Han, Z., Che, Y., Kong, D., Zhao, Q., Han, Z., He, Z.X., et al. (2017). Nitric oxide releasing hydrogel promotes endothelial differentiation of mouse embryonic stem cells. Acta Biomater. *63*, 190–199.

Que, J., Lian, Q., El Oakley, R.M., Lim, B., and Lim, S.K. (2007). PI3 K/Akt/mTOR-mediated translational control regulates proliferation and differentiation of lineage-restricted RoSH stem cell lines. J. Mol. Signal. *2*, 9.

Roggia, C., Ukena, C., Böhm, M., and Kilter, H. (2007). Hepatocyte growth factor (HGF) enhances cardiac commitment of differentiating embryonic stem cells by activating PI3 kinase. Exp. Cell Res. *313*, 921–930.

Seldin, D.C., Landesman-Bollag, E., Farago, M., Currier, N., Lou, D., and Dominguez, I. (2005). CK2 as a positive regulator of Wnt signalling and tumourigenesis. Mol. Cell. Biochem. *274*, 63–67.

Shoemaker, J.E., Lopes, T.J., Ghosh, S., Matsuoka, Y., Kawaoka, Y., and Kitano, H. (2012). CTen: a web-based platform for identifying enriched cell types from heterogeneous microarray data. BMC Genomics *13*, 460.

Shu, T., Liu, C., Pang, M., He, L., Yang, B., Fan, L., Zhang, S., Wang, X., Liu, B., and Rong, L. (2018). Salvianolic acid B promotes neural differentiation of induced pluripotent stem cells via PI3K/AKT/GSK3β/β-catenin pathway. Neurosci. Lett. *671*, 154–160.

Siddle, K. (2011). Signalling by insulin and IGF receptors: supporting acts and new players. J. Mol. Endocrinol. *47*, R1–R10.

Singh, A.M., Reynolds, D., Cliff, T., Ohtsuka, S., Mattheyses, A.L., Sun, Y., Menendez, L., Kulik, M., and Dalton, S. (2012). Signaling network crosstalk in human pluripotent cells: a Smad2/3-regulated switch that controls the balance between self-renewal and differentiation. Cell Stem Cell *10*, 312–326.

Sommercorn, J., Mulligan, J.A., Lozeman, F.J., and Krebs, E.G. (1987). Activation of casein kinase II in response to insulin and to epidermal growth factor. Proc. Natl. Acad. Sci. USA *84*, 8834–8838.

Song, D.H., Sussman, D.J., and Seldin, D.C. (2000). Endogenous protein kinase CK2 participates in Wnt signaling in mammary epithelial cells. J. Biol. Chem. *275*, 23790–23797.

Tabar, V., and Studer, L. (2014). Pluripotent stem cells in regenerative medicine: challenges and recent progress. Nat. Rev. Genet. *15*, 82–92.

Thomson, J.A., Itskovitz-Eldor, J., Shapiro, S.S., Waknitz, M.A., Swiergiel, J.J., Marshall, V.S., and Jones, J.M. (1998). Embryonic stem cell lines derived from human blastocysts. Science *282*, 1145–1147.

Wang, L.G., Liu, X.M., Wikiel, H., and Bloch, A. (1995). Activation of casein kinase II in ML-1 human myeloblastic leukemia cells requires IGF-1 and transferrin. J. Leukoc. Biol. *57*, 332–334.

Wang, L., Schulz, T.C., Sherrer, E.S., Dauphin, D.S., Shin, S., Nelson, A.M., Ware, C.B., Zhan, M., Song, C.Z., Chen, X., et al. (2007). Self-renewal of human embryonic stem cells requires insulin-like growth factor-1 receptor and ERBB2 receptor signaling. Blood *110*, 4111–4119.

Witty, A.D., Mihic, A., Tam, R.Y., Fisher, S.A., Mikryukov, A., Shoichet, M.S., Li, R.K., Kattman, S.J., and Keller, G. (2014). Generation of the epicardial lineage from human pluripotent stem cells. Nat. Biotechnol. *32*, 1026–1035.

Wu, Y., Zhu, R., Zhou, Y., Zhang, J., Wang, W., Sun, X., Wu, X., Cheng, L., Zhang, J., and Wang, S. (2015). Layered double hydroxide nanoparticles promote self-renewal of mouse embryonic stem cells through the PI3K signaling pathway. Nanoscale *7*, 11102–11114.

Ying, H., Kimmelman, A.C., Lyssiotis, C.A., Hua, S., Chu, G.C., Fletcher-Sananikone, E., Locasale, J.W., Son, J., Zhang, H., Coloff, J.L., et al. (2012). Oncogenic Kras maintains pancreatic tumors through regulation of anabolic glucose metabolism. Cell *149*, 656–670.

Yu, J.S., and Cui, W. (2016). Proliferation, survival and metabolism: the role of PI3K/AKT/mTOR signalling in pluripotency and cell fate determination. Development *143*, 3050–3060.

Zhang, H., Badur, M.G., Divakaruni, A.S., Parker, S.J., Jäger, C., Hiller, K., Murphy, A.N., and Metallo, C.M. (2016). Distinct Metabolic States Can Support Self-Renewal and Lipogenesis in Human Pluripotent Stem Cells under Different Culture Conditions. Cell Rep. *16*, 1536–1547.

Zhao, Q., Feng, Y., Zhu, Z., and Dimitrov, D.S. (2011). Human monoclonal antibody fragments binding to insulin-like growth factors I and II with picomolar affinity. Mol. Cancer Ther. *10*, 1677–1685.

Zhao, J., Cao, H., Tian, L., Huo, W., Zhai, K., Wang, P., Ji, G., and Ma, Y. (2017). Efficient Differentiation of TBX18^{+}/WT1^{+} Epicardial-Like Cells from Human Pluripotent Stem Cells Using Small Molecular Compounds. Stem Cells Dev. *26*, 528–540.

STAR★METHODS

KEY RESOURCES TABLE

REAGENT or RESOURCE	SOURCE	IDENTIFIER
Antibodies		
Non-phospho (Active) β-Catenin (Ser33/37/Thr41) Antibody	Cell Signaling	Cat# 4270; RRID:AB_1903918
Dvl Antibody (B-4)	Santa Cruz	Cat# sc-166303; RRID:AB_2093321
Histone H3 Antibody	Cell Signaling	Cat# 9715; RRID:AB_331563
Phospho-Akt (Ser473) Antibody	Cell Signaling	Cat# 9271; RRID:AB_329825
CSNK2A1 Antibody	DSHB	Cat# AFFN-CSNK2A1-5F1; RRID:AB_2617527
Phospho-GSK-3α/β (Ser21/9) Antibody	Cell Signaling	Cat# 9331; RRID:AB_329830
GAPDH Antibody (FL-335)	Santa Cruz	Cat# sc-25778; RRID:AB_10167668
IGF Antibody	From Zhao lab (Zhao et al., 2011)	N/A
Her2 Antibody	From Zhao lab (Harries and Smith, 2002)	N/A
8H9 Antibody	From Zhao lab (Ahmed et al., 2015)	N/A
Human IGF-II/IGF2 Antibody	R&D	Cat# MAB292
TNNT2 Antibody	DSHB	Cat# CT3; RRID:AB_528495
Nkx-2.5 Antibody (H-114)	Santa Cruz	Cat# sc-14033; RRID:AB_650281
NKX2-5 Antibody	DSHB	Cat# PCRP-NKX2-5-1E6; RRID:AB_2618895
MEF2C (D80C1) XP® Rabbit mAb	Cell Signaling	Cat# 5030; RRID:AB_10548759
Monoclonal Anti-α-Actinin (Sarcomeric) Antibody	Sigma	Cat# a7811; RRID:AB_476766
Recombinant Anti-Wilms Tumor Protein Antibody	Abcam	Cat# ab89901; RRID:AB_2043201
Recombinant Anti-alpha smooth muscle Actin Antibody [E184]	Abcam	Cat# ab32575; RRID:AB_722538
Alpha-1-Fetoprotein Antibody	Dako	Cat# A0008; RRID:AB_2650473
VE-cadherin (CDH5) Antibody (F-8)	Santa Cruz	Cat# sc-9989; RRID:AB_2077957
CD44 Alexa Fluor 488 Conjugate Kit	Molecular probes	Cat# A25528; RRID: N/A
PDGF Receptor α Antibody	Cell signaling	Cat# 3164; RRID:AB_2162351
Anti-VEGF Receptor 2 (KDR) Antibody	Abcam	Cat# Ab2349; RRID:AB_302998
Peroxidase AffiniPure Goat Anti-Mouse IgG (H+L)	Jackson	Cat# 115-035-146; RRID:AB_2307392
Peroxidase AffiniPure Goat Anti-Rabbit IgG (H+L)	Jackson	Cat# 111-035-144; RRID:AB_2307391
Alexa Fluor® 488 AffiniPure Goat Anti-Mouse IgG	Jackson	Cat# 115-545-071; RRID:AB_2307391
Alexa Fluor® 647 AffiniPure Goat Anti-Rabbit IgG	Jackson	Cat# 111-605-046; RRID:AB_2338076
Alexa Fluor® 488 AffiniPure Goat Anti-Rabbit IgG	Jackson	Cat# 111-545-046; RRID:AB_2338050
Bacterial and Virus Strains		
Lentivirus for plasmid transduction	Generated by standard methods using packaging plasmids pMD2.G and psPAX2	N/A
Chemicals, Peptides, and Recombinant Proteins		
L-ascorbic acid-2-phosphate magnesium	Sigma	Cat# A8960
Sodium selenium	Sigma	Cat# S5261
holo-transferrin human	Sigma	Cat# T0665
bFGF	From Chen lab (Chen et al., 2012)	N/A
Recombinant human TGF-β1	Peprotech	Cat# 100-21
Insulin solution human	Sigma	Cat# I9278
Sodium bicarbonate	Sigma	Cat# S5761

(*Continued on next page*)

Continued

REAGENT or RESOURCE	SOURCE	IDENTIFIER
Sodium chloride	Sigma	Cat# S5886
Chloroform	Sinopharm Chemical	N/A
2-Propanol	Sigma	Cat# I9516
Ethanol absolute	Merck	Cat# 102428
DNase/RNase-free distilled water	Invitrogen	Cat# 10977023
Tris (hydroxymethyl) aminomethane	Sangon	Cat# A600194
Sodium dodecyl sulfate	Sigma	Cat# L4509
Glycerol	Sangon	Cat# A600232
β-mercaptoethanol	Sigma	Cat# M6250
Bromophenol blue	Sigma	Cat# B0126
Potassium chloride	Sigma	Cat# P5405
Magnesium chloride	Sigma	Cat# M4880
Paraformaldehyde	Sigma	Cat# P6418
Recombinant Human/Mouse/Rat Activin A Protein	R&D	Cat# 338-AC-050/CF
Recombinant Human BMP-4 Protein	R&D	Cat# 314BP
Y-27632 2HCl	Selleck	Cat# S1049
RKI-1447	Selleck	Cat# S7195
CHIR-99021	Selleck	Cat# S1263
IWP-2	Selleck	Cat# S7085
LY294002	Selleck	Cat# S1105
Wortmannin	Santa Cruz	Cat# sc-3505
PI-103	Selleck	Cat# S1038
Silmitasertib (CX-4945)	Selleck	Cat# S2248
Apigenin	Sigma	Cat# 10798
Dimethyl sulfoxide	Sigma	Cat# D4540
Puromycin dihidrochloride	Fisher Scientific	Cat# BP2956-100
Critical Commercial Assays		
Seahorse XF Cell Mito Stress Test kit	Agilent	Cat# 103015-100
Deposited Data		
Microarray data	This paper	GEO: GSE139625
Experimental Models: Cell Lines		
Human ESC H1	Thomson et al., 1998	N/A
Human ESC H9	Thomson et al., 1998	N/A
iPSC NL-4 (NCRM-4)	From NIH	N/A
HEK293-FT	ATCC	Cat# PTA-5077, RRID:CVCL_6911
Experimental Models: Organisms/Strains		
Tg(Fli1:EGFP) transgenic zebrafish	Ai et al., 2018	N/A
Oligonucleotides		
Primers used for real-time qPCR, see Table S1	This paper	N/A
CSNK2A1 shRNA-1 target sequence: AGAATTTGAGAGGAGGTCCCA	This paper	N/A
CSNK2A1 shRNA-2 target sequence: CGTAAACAACACAGACTTCAA	This paper	N/A
Recombinant DNA		
pMD2.G	Gift from Didier Trono	Addgene plasmid # 12259; RRID: Addgene_12259
psPAX2	Gift from Didier Trono	Addgene plasmid # 12260; RRID: Addgene_12260

(*Continued on next page*)

Continued

REAGENT or RESOURCE	SOURCE	IDENTIFIER
Software and Algorithms		
Microsoft Excel	Microsoft Office	https://products.office.com/en-us/?rtc=1
Microsoft PowerPoint	Microsoft Office	https://products.office.com/en-us/?rtc=1
Prism 8	GraphPad Software	https://www.graphpad.com
ImageJ	ImageJ	https://imagej.nih.gov/ij/
FlowJo V10	FlowJo	https://www.flowjo.com
ZEN Microscope Software	ZEISS	https://www.zeiss.com/corporate/int/home.html
R 3.4.2	R Software	https://www.r-project.org/
Other		
Microarray data	Lin et al., 2017	GEO accession number GSE81711
Matrigel, growth factor reduced	Corning	Cat# 354230
DMEM/F12	GIBCO	Cat# 11330057
Chemically defined lipid concentrate	GIBCO	Cat# 11905031
RNAiso Plus	Takara	Cat# 9101
cDNA reverse transcription kit	Applied Biosystems	Cat# 4368813
SYBR premix Ex Taq	Takara	Cat# RR420A
TERGITOL solution	Sigma	Cat# NP40S
Triton X-100	Sigma	Cat# X100
Super Signal West Dura Extended Duration Substrate	Thermo	Cat# 34076
TrypLE select enzyme	Life	Cat# 12563
Fetal bovine serum	GIBCO	Cat# 10270106
Bovine Serum Albumin	Sigma	Cat# A7030
EDTA (0.5 M), pH 8.0	Ambion	Cat# AM9262
PBS	GIBCO	Cat# 70011
HEPES	Sigma	Cat# H4043
UPLC BEH amide column (100 mm × 2.1 mm i.d., 1.7 μm)	Waters	Cat.# 186004801

LEAD CONTACT AND MATERIALS AVAILABILITY

Further information and requests for resources and reagents should be directed to and will be fulfilled by the Lead Contact, Dr. Guokai Chen, guokaichen@um.edu.mo. This study did not generate new unique reagents.

EXPERIMENTAL MODEL AND SUBJECT DETAILS

Ethics Statement

The use of hESCs and hiPSCs were approved by the Institutional Review Board at the University of Macau. Zebrafish were handled according to the Animal Protection Act enacted by the Legislative Council of Macao Special Administrative Region under Article 71(1) of the Basic Law, and the experimental protocols were approved by the Research Ethics Committee of the University of Macau.

Cell Lines

Most experiments were done on H1 hESC line. H9 hESC and NL-4 hiPSC lines were also used to confirm key findings. The cells were cultured in E8 medium on matrigel coated surface (Chen et al., 2011), and the cells were passaged with EDTA/DPBS buffer every 3-4 days following standard procedure (Beers et al., 2012).

Zebrafish

Tg(Fli1:EGFP) transgenic zebrafish was used in the study. Zebrafish care and maintenance and treatment of zebrafish larvae were carried out as previous described (Ai et al., 2018). 16-18 hpf embryos were subjected to different treatments. Photos were taken between 96 hpf to 120 hpf.

METHOD DETAILS

Mesoderm induction and subsequent differentiation

The differentiation procedure was performed as shown in Figure 1A. hESCs were passaged 2 days before differentiation, and differentiation was initiated when the culture confluency reached around 70%. All differentiation experiments were conducted in differentiation basal medium (DMEM/F12, L-ascorbic acid-2-phosphate magnesium (64 μg/mL), sodium selenite (14 ng/ml), holo-transferrin (10 μg/mL), chemically defined lipid concentrate (1x)). On Day 0, CHIR99021 (5 μM) was applied on hESCs to initiate mesoderm differentiation in basal medium; from Day 1 to Day 10, cells were cultured in basal medium, and different treatments were applied according to specific experimental design. For cardiac differentiation, the treatments were applied between Day 2 and Day 5 unless otherwise specified. In order to better analyze the effects of IGF or CK2 inhibition between Day 2 and Day 5, 1 μg/ml insulin was added from day 0 to day 2 to decrease spontaneous cardiomyocyte differentiation unless otherwise specified. After Day 5, insulin (10 μg/mL) was added to the culture to help cell proliferation.

Endoderm differentiation

Endoderm differentiation was conducted in E8 medium supplemented with 1% BSA. hESCs were treated with CHIR99021 (5 μM) from day 0 to day 1, and then with activin A (10 ng/mL) from Day 1 to Day 4; additional drugs were applied between Day 1 and Day 4. Samples were harvested for analysis on Day 4.

Reverse transcription and real-time quantitative PCR

Total RNA was extracted from adherent cells by RNAiso Plus (Takara, 9109). The reverse transcription was conducted using High-Capacity cDNA Reverse Transcription Kit from Applied Biosystems (Thermo, 4368814) following the protocol recommended by the manufacturer. Real-time qPCR was conducted in 384-well high throughput format using Takara SYBR® Premix Ex Taq II on Applied Biosystems QuantStudio 7 Flex Real-time PCR System following the protocol recommended by the manufacturer. The analysis was conducted by the ΔΔCT method. For each analysis, the mRNA level was normalized to the levels of housekeeping gene GAPDH.

Western blot

Whole cell protein extracts were harvested with laemmli sample buffer. Nuclear fraction extraction was performed as previously described (Dignam et al., 1983; Gustafsson Sheppard et al., 2015). Proteins were separated by SDS-PAGE, transferred onto PVDF membranes, and incubated with primary and secondary antibodies. Signals were detected using Super Signal West Dura Extended Duration Substrate (ThermoFisher, 34076).

Flowcytometric analysis

For flow cytometric analysis, cells were washed with PBS, detached with TrypLE select enzyme for 10 min at 37°C, neutralized with an equal volume of 5% FBS medium, and then pelleted by centrifugation at 500 × g for 5 min. Cells were resuspended and fixed with 4% paraformaldehyde for 15 min at room temperature. Subsequently, the fixed cells were washed twice with PBS and permeabilized in 0.4% Triton X-100 containing blocking buffer (PBS with 1% BSA) for 30 min at room temperature. The fixed cells were either stored at 4°C for up to 2 weeks or directly analyzed. The cells were stained with primary antibody diluted in PBS overnight at 4°C, washed twice with PBS, and incubated with secondary antibody for 1 h at room temperature. Finally, the cells were washed three times with PBS to remove the secondary antibody. The fluorescent flow cytometric analysis was conducted using a BD Biosciences AccuriC6 flowcytometer. The data were analyzed by Flowjo software.

Immunocytochemistry

For immunofluorescence imaging, the adherent cells were washed with PBS and directly fixed with 4% PFA for 15 min at room temperature. The fixed cells were washed once with PBS and permeabilized in 0.4% Triton X-100 containing blocking buffer for 30 min at room temperature. Subsequently, the cells were stained with primary antibodies diluted in PBS overnight at 4°C, washed twice with PBS, and incubated with secondary antibodies for 1 h at room temperature. The secondary antibodies were then removed by washing three times with PBS, and the cells were incubated with Hoechst for 15 min at room temperature. The cells were washed to removed excess Hoechst and mounted in mounting medium prior to imaging. The images were captured with Carl Zeiss Axio Observer or EVOS® FL Cell Imaging System.

Microarray analysis

Total RNA was extracted using RNAiso Plus (Takara), and reverse-transcribed to cRNA using SuperScript III kit and TargetAmp-Nano Labeling Kit (Epibio) following the manufacturer's protocol. Sample hybridization was carried out using the HumanHT-12 v4 Expression BeadChip Kit (Illumina). The arrays were scanned using iScanner (Illumina). Functional annotation was performed through Database for Annotation, Visualization, and Integrated Discovery (DAVID) version 6.7. Cell type analysis was performed using Cell Type Enrichment Analysis (CTen) (Shoemaker et al., 2012), DAVID and Enrichr (Chen et al., 2013; Kuleshov et al., 2016). Genes with a fold change $\geq$ 1.5 or 2 were considered significantly differentially expressed. Heatmap for transcriptomics data was performed using the Pheatmap R package.

Quantification of intracellular metabolic products

The intracellular metabolic products were determined by LC-MS/MS. Samples were prepared according to previous publication (Ying et al., 2012; Zhang et al., 2016). The metabolic profile was obtained with Waters ACQUITYTM UPLC system coupled with a Waters Xevo TQD Triple Quadrupole Mass Spectrometry (Waters Corp., Milford, USA). UPLC BEH amide column (100 mm × 2.1 mm i.d., 1.7 μm) was used for the determination. The quantification was normalized by cellular protein content.

Electrophysiology analysis

Cells and material preparation are based on previous publication (Long et al., 2013). Patch clamp recordings were performed using an Axopatch 200B patch clamp amplifier with a Digidata 1400 interface (Axon Instruments, USA). A Flaming/Brown micropipette puller (P-97; Sutter Instruments Co.) was used to fabricate patch pipettes from a capillary glass. Patch pipette resistances were 2–4 MΩ by establishing a gigaohm seal and recording using the traditional ruptured patch approach. Data were acquired and analyzed using pCLAMP programs (10.0; Axon Instruments).

Seahorse analysis

Mito Stress Test was carried out using Seahorse XF Cell Mito Stress Test kit on XFe96 Extracellular Flux Analyzer (Seahorse Biosciences) following manufacturer's protocol. The cardiomyocytes cells generated by different methods were seeded in the Matrigel precoated plates to tests. After the tests, cells were lysed in well with 0.1% Trition X-100 solution (0.1% triton, 10 mM Tris-HCl) followed by Bradford quantification. The final values were normalized to absorbance at 595nm.

shRNA knockdown

CSNK2A1 shRNA constructs were obtained from Fulengen, Inc. Two constructs were designed for *CSNK2A1* knockdown.: CSNK2A1 shRNA-1 target sequence: AGAATTTGAGAGGAGGTCCCA. CSNK2A1 shRNA-2 target sequence: CGTAAACAACACA GACTTCAA. pLKO.1-TRC control plasmid was used as negative control. The lentivirus was packaged in 293FT cells with psPAX2 and pMD2.G (https://www.addgene.org/protocols/plko/). Fresh differentiation basal medium was used to collect virus. Virus-containing medium was harvested at 48 hours and 72 hours after transfection, and stored at −80°C before transduction. The virus was added together with 5 μg/ml polybrene from day 2 to day 3 of the neutral differentiation. 1 μg/ml puromycin was applied for selection from day 10. The cells were harvested for analysis on day 14.

QUANTIFICATION AND STATISTICAL ANALYSIS

The bar charts were generated using GraphPad Prism 8. The heatmaps were generated using R 3.4.2 software. The quantification of the immunoblot was performed by ImageJ.

Statistical analyses were carried out by unpaired two-tailed Student's t test using Microsoft Excel. $p < 0.05$ was considered statistically significant (*). Statistical details of experiments, including the value and meaning of n, can be found in the figure legends. Data are shown as mean ± SD unless specified otherwise.

DATA AND CODE AVAILABILITY

The GEO accession number for the microarray data reported in this study is GEO: GSE139625. The GEO accession number for the microarray data from Lin et al. is GEO: GSE81711.